# Evaluation and validation of equivalent properties of macro fibre composites for piezoelectric transducer modelling

Yang Kuang and Meiling Zhu*

*Corresponding author: m.zhu@exeter.ac.uk

College of Engineering, Mathematics and Physical Sciences, University of Exeter, Exeter, EX4 4QF, UK

## Abstract

Piezoelectric transducers based on macro fibre composites (MFCs) are widely used for energy harvesting, actuation and sensing because of the high conformability, reliability and strong piezoelectric effect of MFCs. Analytical or numerical modelling of the heterogeneous MFC as a homogenous material with equivalent properties is usually required to predict the performance of the transducers. However, the equivalent properties reported in the literature are not suitable for this purpose. This work proposes an equal power-output method to numerically evaluate the equivalent properties of $d_{31}$ type MFCs for piezoelectric transducer modelling. Taking energy harvesting application as a study case, it departs from the traditional method by applying electric assumptions that ensure the equal voltage, electric charge, and thus equal power output between the heterogeneous and homogeneous MFCs. The equivalent properties were characterised through the finite element (FE) analysis of the MFC's representative volume element (RVE), which is the minimum periodic unit in the MFC and takes account all the constitutes. The validity of these equivalent properties for energy harvesting transducer modelling was verified by FE modelling as well as experimental testing. The application of the equivalent properties for actuation and sensing transducer modelling was analysed and validated. FE modelling results showed that a homogeneous RVE with the equivalent properties accurately simulated the energy harvesting and actuation behaviours of the heterogeneous RVE. The simulated power output of MFC-based strain energy harvesters matched the mean experimental results with a mean error of 2.5%. When used for actuation, the MFC produced a free strain of 0.93 $\mu\varepsilon/V$, which is close to the manufacturer specification.

**Keywords**: macro-fibre composite (MFC); energy harvesting; equivalent properties; finite element modelling; homogenization

## 1. Introduction

Piezoelectric transducers for energy harvesting [1, 2], actuation [3, 4] and sensing [5] are well-established applications of piezoelectric materials. The most commonly used piezoelectric materials for these applications are piezoelectric ceramics, polymers and composites. Piezoelectric ceramics, mainly PZT, have excellent piezoelectric properties and thus high efficiency in energy transduction. However, their extremely brittle nature limits their conformability to curved surfaces and the stress/strain they can safely withstand without damage [6, 7]. Piezoelectric polymers, mainly polyvinylidene difluoride (PVDF), can sustain much higher strain than ceramics due to their intrinsic flexibility [8, 9], but the weak piezoelectric effect severely restricts the performance of PVDF in application. Piezoelectric composites comprise a piezoelectric fibrous phase embedded in an epoxy matrix phase. One of the most successful such composites is macro fibre composite (MFC), which was developed by NASA and is produced by Smart Materials Corp. It consists of rectangular PZT fibres embedded in an epoxy matrix and sandwiched between two electrode/epoxy layers. The whole structure is then encapsulated by two Kapton layers. It holds high strength, flexibility and reliability while still maintain a strong piezoelectric effect, thus attracting great interests for industrial applications and in the academic community [10-13].

Analytical or numerical analyses are usually required to predict and optimise the performance of piezoelectric transducers. For MFC-based transducers, considering the detailed structure of MFC will lead to enormous complexity of the analytical and numerical models. A practical approach is to envisage the heterogeneous MFC as a homogeneous piezoelectric material assigned with equivalent material properties. However, because of the complex structure of MFCs, the determination of the equivalent elastic and electro-mechanical properties of the MFC is challenging and the manufacturer

has provided only limited information [14]. This challenge has attracted a great deal of effort in the research community [15-17].

Various homogenisation techniques have been developed to determine the equivalent properties of the MFCs, such as analytical mixing rules [15, 18, 19], asymptotic homogenisation [20] and finite element (FE) homogenization. Deraemaeker *et al.* [15] proposed analytical mixing rules based on uniform field method to determine the equivalent properties of the active layer (PZT fibers embedded in epoxy matrix) of the MFC. Prasath *et al.* extended the application of the analytic mixing rules from the active layer [18] to the whole MFC including all the layers [19]. An asymptotic expansion homogenization method [20] was applied to compute the effective properties of $d_{31}$ type MFC and showed comparable results with the analytical mixing rules. While the analytical methods become complex when considering all the layers of the MFC, FE analysis of MFC's representative volume element (RVE) [19, 21-23] provides a good solution. It is applicable to general geometries and has been successfully applied to $d_{31}$, $d_{33}$ and $d_{15}$ type MFCs. A common feature of these homogenisation methods is that they are all based on average quantities, i.e. the four field variables (electric field, electric displacement, stress and strain) of the homogeneous MFC are calculated as the volume-average of their counterparts in the heterogeneous MFC. They mainly differ in the techniques to determine these average quantities. For analytical mixing rules, the four field variables are assumed to be uniform within each constitute of the MFC. In case of an independent field variable, it is equal in each constitute and also equal to the corresponding average quantity. In case of a dependent field variable, the average quantity is a linear combination of the field variable in each constitute in terms of volume fraction. For FE homogenization, the field variables in a heterogeneous RVE subjected to specially designed boundary conditions are simulated and then averaged over the volume to derive the average quantities.

The aforementioned homogenisation techniques result in relatively consistent equivalent properties and they have been successfully used to understand the global behaviours of MFCs [15-17] as well as their dependence on various parameters such as fibre volume fraction [19, 24], bonding layer [25] and electric field strength [23]. However, as pointed out in [26, 27], the equivalent piezoelectric and dielectric constants are dependent on the arbitrary chosen electrical assumption and boundary conditions. For these homogenization methods, the electric assumption is that the electric field and electric displacement of the homogeneous MFC is the volume-average quantities over the active layer [19, 25] or the whole MFC [23, 26, 27]. The equivalent properties of the $d_{31}$ MFC evaluated under this electric assumption may be difficult to use for transducer modelling, because the electric assumption has considered the equality or equivalent of the electric field and displacement, but not the equality of the voltage and electric charge between the heterogeneous and homogenous MFCs. For instance, in [23, 26, 27], the electric displacement of the homogeneous MFC was calculated by averaging the electric displacement produced solely by the PZT fibres over the whole MFC volume. Consequently, the electric displacement of the homogenous MFC, which is also the electric charge density, would be smaller than the heterogeneous. As a result, the homogenous MFC would have less electric charge than the heterogeneous. This could further lead to the inequality of other macroscopic parameters, e.g. voltage and electric power output for energy harvesting transducers. Steiger and P. Mokrý [28] have also found that when the MFC actuator is modelled as a homogenous piezoelectric material with identical geometrical dimensions, the $d_{31}$ should be -267 pC/m. This value of $d_{31}$ is significantly larger than the equivalent values (~-170 pC/m) reported in the literatures using the aforementioned electric assumptions [19] [23].

This work proposes an equal power-output method for the first time to evaluate the equivalent properties of $d_{31}$ type MFC for transducer modelling. It departs from the traditional method by applying electric assumptions that ensure the equal voltage, electric charge, and thus equal power output between the heterogeneous and homogeneous MFCs. Energy harvesting application is used as a study case. Finite element analysis of the RVE is performed to evaluate the equivalent properties, which are validated by FE modelling and experimental measurement of a strain energy harvester. The application of the equivalent properties for actuation and sensing is also analysed and validated. The methodology developed can also be used to evaluate the equivalent properties of other piezoelectric composites for transducer modelling.

## 2. Homogenization of MFCs: taking energy harvesting as a study case

A schematic of the $d_{31}$ type MFC is shown in Fig. 1 (a). The MFC consists of 5 layers: an active layer with PZT fibres embedded in an epoxy matrix, two electrode layers with copper and epoxy phases, and two protective layers of Kapton. The PZT fibres are polled along 3-axis and metallized on surfaces normal to the 3-axis. Modelling the heterogeneous MFC directly is unwise because of the high computational cost due to the highly complex microstructure. An alternative way is to model the heterogeneous MFC as a homogeneous material, which has the same dimensions as the heterogeneous MFC and is assigned with equivalent macroscopic properties. The homogeneous MFC consists of a single layer of piezoelectric material polled along 3-axis, as shown in Fig. 1 (b).

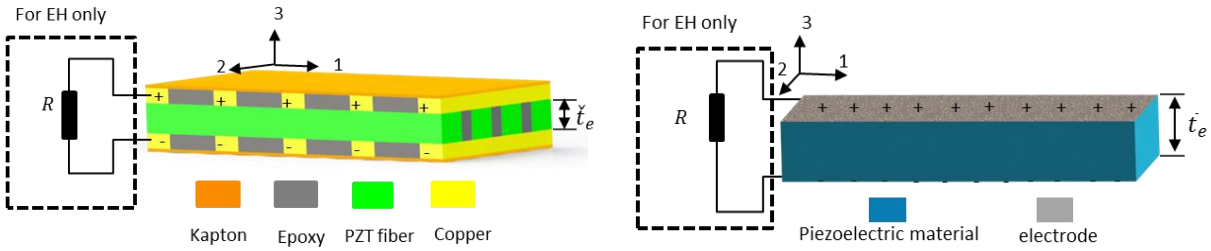


(a) (b)

Fig. 1 A schematic of (a) a real $d_{31}$-type MFC, which is heterogeneous and (b) the homogeneous MFC. The load resistors $R$ in the dashed boxes are for energy harvesting applications.

The homogenization of the MFC is to evaluate the equivalent properties, with which the homogeneous MFC generates equal outputs of interest as the heterogeneous MFC when the same inputs are applied. The behaviours of the homogeneous MFC should comply with the constitutive equation of piezoelectric material, the stress-charge form of which is

$$\begin{Bmatrix} \bar{T}_1 \\ \bar{T}_2 \\ \bar{T}_3 \\ \bar{T}_4 \\ \bar{T}_5 \\ \bar{T}_6 \\ \bar{D}_3 \end{Bmatrix} = \begin{bmatrix} \bar{c}_{11}^E & \bar{c}_{12}^E & \bar{c}_{13}^E & 0 & 0 & 0 & -\bar{e}_{31} \\ \bar{c}_{21}^E & \bar{c}_{22}^E & \bar{c}_{23}^E & 0 & 0 & 0 & -\bar{e}_{32} \\ \bar{c}_{31}^E & \bar{c}_{32}^E & \bar{c}_{33}^E & 0 & 0 & 0 & -\bar{e}_{31} \\ 0 & 0 & 0 & \bar{c}_{44}^E & 0 & 0 & 0 \\ 0 & 0 & 0 & 0 & \bar{c}_{55}^E & 0 & 0 \\ 0 & 0 & 0 & 0 & 0 & \bar{c}_{66}^E & 0 \\ \bar{e}_{31} & \bar{e}_{32} & \bar{e}_{33} & 0 & 0 & 0 & \bar{\epsilon}_{33}^S \end{bmatrix} \begin{Bmatrix} \bar{S}_1 \\ \bar{S}_2 \\ \bar{S}_3 \\ \bar{S}_4 \\ \bar{S}_5 \\ \bar{S}_6 \\ \bar{E}_3 \end{Bmatrix}. \quad (1)$$

where $\bar{c}_{ij}^E$ with $i,j = 1,\cdots,6$ are the equivalent elastic constants at zero electric field ($\bar{E}_3 = 0$); $\bar{e}_{3p}$ with $p = 1,2,3$ are the equivalent piezoelectric stress constants; $\bar{\epsilon}_{33}^S$ is the equivalent dielectric constant at blocked strain; $\bar{S}_j$, $\bar{T}_j$, $\bar{D}_3$ and $\bar{E}_3$ are the strain, stress, electric displacement and electric field in the homogenous MFC, respectively. It should be noted that the in-plane electric field is omitted ($\bar{E}_1 = \bar{E}_2 = 0$) in Eq. ( 1 ) because the MFC is polled along 3-axis. In this study, symbols with an accent of '¯' and '˘' respectively represent variables for homogeneous and heterogeneous MFCs.

### 2.1. Equal power-requirement for energy harvesting

When MFCs are used for energy harvesting, mechanical deformations are applied and an electric voltage is generated by the PZT fibres, which is dissipated in a load resistor, as shown in Fig. 1. The output of interest for energy harvesting is the electric power output delivered to the load resistor. Therefore, when homogenising the MFC for energy harvesting application, the heterogeneous and homogeneous MFCs must produce equal power output when connected to the same load resistor. To derive the conditions satisfying this equal-power requirement, a circuit model representing a piezoelectric energy harvester (PEH) connected to a load resistor [29, 30] is considered (Fig. 2). In this model, the PEH is envisaged as a voltage source $U_{OC}$ (open-circuit voltage of the PEH) connected in series with the intrinsic capacitor, $C_P$ of the piezoelectric material. Apparently, with the same mechanical input, the heterogeneous and homogeneous MFCs must have equal $U_{OC}$ and $C_P$ so that the equal power-requirement can always be met.

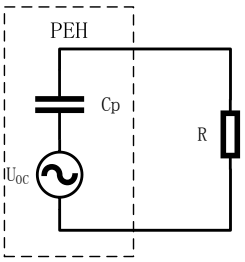


Fig. 2 An equivalent circuit model of the PEH connected to a load resistor

### 2.2 Proposed homogenization method for energy harvesting

Since the conditions that satisfy the equal power-requirement is related to the voltage, capacitance and electric charges, Eq. ( 1 ) is rewritten in terms of these macroscopic variables in Eq. ( 2 ) by incorporating Eq. ( 3 ).

$$\begin{Bmatrix} \bar{T}_1 \\ \bar{T}_2 \\ \bar{T}_3 \\ \bar{T}_4 \\ \bar{T}_5 \\ \bar{T}_6 \\ \bar{Q}_3 \end{Bmatrix} = \begin{bmatrix} \bar{c}_{11}^E & \bar{c}_{12}^E & \bar{c}_{13}^E & 0 & 0 & 0 & -\bar{e}_{31}/\bar{t}_e \\ \bar{c}_{21}^E & \bar{c}_{22}^E & \bar{c}_{23}^E & 0 & 0 & 0 & -\bar{e}_{32}/\bar{t}_e \\ \bar{c}_{31}^E & \bar{c}_{32}^E & \bar{c}_{33}^E & 0 & 0 & 0 & -\bar{e}_{31}/\bar{t}_e \\ 0 & 0 & 0 & \bar{c}_{44}^E & 0 & 0 & 0 \\ 0 & 0 & 0 & 0 & \bar{c}_{55}^E & 0 & 0 \\ 0 & 0 & 0 & 0 & 0 & \bar{c}_{66}^E & 0 \\ \bar{e}_{31}\bar{A}_e & \bar{e}_{32}\bar{A}_e & \bar{e}_{33}\bar{A}_e & 0 & 0 & 0 & \bar{C}_P^S \end{bmatrix} \begin{Bmatrix} \bar{S}_1 \\ \bar{S}_2 \\ \bar{S}_3 \\ \bar{S}_4 \\ \bar{S}_5 \\ \bar{S}_6 \\ \bar{U}_3 \end{Bmatrix} \quad (2)$$

$$\bar{Q}_3 = \bar{D}_3\bar{A}_e, \bar{U}_3 = \bar{E}_3\bar{t}_e, \bar{C}_P^S = \frac{\bar{\epsilon}_{33}^S\bar{A}_e}{\bar{t}_e} \quad (3)$$

where $\bar{A}_e$ and $\bar{t}_e$ are the electrode area and distance of the homogeneous MFC, respectively; $\bar{Q}_3$ and $\bar{U}_3$ are the electrical charge collected on and the voltage across the electrodes of the homogenous MFC. $\bar{C}_P^S$ is the clamped capacitance of the homogenous MFC.

The behaviours of the homogenous MFC must comply with Eq. ( 2 ). To determine the equivalent parameters, the stress $\bar{T}_j$, strain $\bar{S}_j$, electrical charge $\bar{Q}_3$ and voltage $\bar{U}_3$ of the homogenous MFC should be first calculated based on the corresponding variables in the heterogeneous one so that Eq. ( 2 ) can then be solved. The stress $\bar{T}_j$ and strain $\bar{S}_j$ of the homogeneous MFC are determined by using the traditional average quantity method as

$$\bar{T}_j = \frac{1}{V_o}\int_{V_o} \check{T}_j dV_o \ , \quad \bar{S}_j = \frac{1}{V_o}\int_{V_o} \check{S}_j dV_o \quad (4)$$

where $\check{T}_j$ and $\check{S}_j$, $j = 1,2\cdots 6$ are the local stress and strain in the heterogeneous MFC; $V_o$ is the volume of the MFC.

To ensure equal open-circuit voltage between the homogenous and heterogeneous MFC, the voltage $\bar{U}_3$ is calculated by

$$\bar{U}_3 = \check{U}_3, \quad (5)$$

where $\check{U}_3$ is voltage produced by the heterogeneous MFC. Eq. ( 5 ) ensures that the heterogeneous and homogenous MFCs always produce the same voltage at any conditions and thus they share the same open-circuit voltage.

The capacitance $C_P$ in Fig. 2 depends on the stress/strain boundary conditions. The $C_P$ of a piezoelectric material under constant strain condition can be evaluated by applying a voltage to the piezoelectric material while blocking the strain in the three normal directions (to exclude the generation of electric charges by mechanical strain through piezoelectric effect). The ratio of the measured electric charge to the applied voltage is the value of $C_P$. For the homogenous MFC, the expression of $\bar{C}_P$ under constant strain condition ($\bar{S}_1, \bar{S}_2$ and $\bar{S}_3$ are fixed), can be derived by applying the blocked strain boundary condition, i.e. $\bar{S}_1 = \bar{S}_2 = \bar{S}_3 = 0$ to Eq. ( 2 ).

$$\bar{C}_P = \frac{\bar{Q}_3}{\bar{U}_3} = \frac{\bar{\epsilon}_{33}^S\bar{A}_e}{\bar{t}_e} = \bar{C}_P^S \quad (6)$$

$\bar{Q}_3$ in Eq. ( 6 ) is the electric charge produced due to the voltage $\bar{U}_3$, i.e. without contribution from mechanical strain.

Under the same blocked strain condition ($\bar{S}_1 = \bar{S}_2 = \bar{S}_3 = 0$), the capacitance of the heterogeneous can be calculated by the ratio of the electric charges $\check{Q}_3$ produced due to an applied voltage $\check{U}_3$ to $\check{U}_3$:

$$\check{C}_P = \frac{\check{Q}_3}{\check{U}_3} \quad (7)$$

It is worthwhile pointing out that the blocked/constant strain condition of the heterogeneous MFC should be attained by constraining the boundary surface displacements of the whole MFC, not by constraining the displacement of all constitutes. If all constitutes are constrained in displacement, then the interaction between different constitutes in the MFC will be

blocked and thus will not reflect the behaviour of the MFC. When the displacement constraint is applied to the boundary surface of the MFC to achieve the blocked strain condition, the strain in the PZT fibres is not entirely blocked. Under such a condition, when a voltage $\breve{U}_3$ is applied on the heterogonous MFC, on one hand, electric charges are produced through the dielectric constant of the PZT fibre; on the other hand, the voltage will causes a strain in the PZT fibres, which in return produces electric charges through direct piezoelectric effect. As a result, the ratio of $\breve{Q}_3$ to $\breve{U}_3$ is not only related to the dielectric constant, but also related to the piezoelectric effect. In other words, $\breve{C}_P$ is not the clamped capacitance of the PZT fibres ($\breve{\epsilon}_{33}^S \breve{A}_e/\breve{t}_e$), although $\bar{C}_P$ is the clamped capacitance of the homogenous MFC ($\bar{\epsilon}_{33}^S \bar{A}_e/\bar{t}_e$).

Combining Eqs. (5-7), the condition for the equal capacitance under a constant strain condition is

$$\bar{Q}_3 = \breve{Q}_3 \tag{8}$$

Eqs. ( 5 ) and ( 8 ), which are always maintained, defines the electrical assumption of the homogenization process and ensures that the heterogeneous and homogenous MFCs always produce equal electrical charge and voltage at any circuit conditions. As a result, they produce equal open-circuit voltage and have equal capacitance, satisfying the equal power-requirement. It should be noted that while the voltages of heterogeneous and homogenous MFCs are kept equal by Eq. (7), the electric field will be different because of the different electrode distances.

## 3. Evaluating the equivalent properties by FE analysis of the RVE

The homogenization method proposed in section 2 can be implemented both numerically and analytically. In this study, a finite element approach is used because of the advantages mentioned in the introduction.

### 3.1 FE modelling of the RVE of the MFC

The FE modelling of RVE has been widely used to evaluate the equivalent properties of piezoelectric composites [16-18, 21, 31]. The RVE is a through-thickness cut of the MFC and represents the minimum periodic unit, as shown in Fig. 3. It has a section of the PZT fibre sandwiched between two copper/epoxy layers which are covered by two protective Kapton layers. The MFC can be envisaged as a periodic array of RVEs without any overlap.

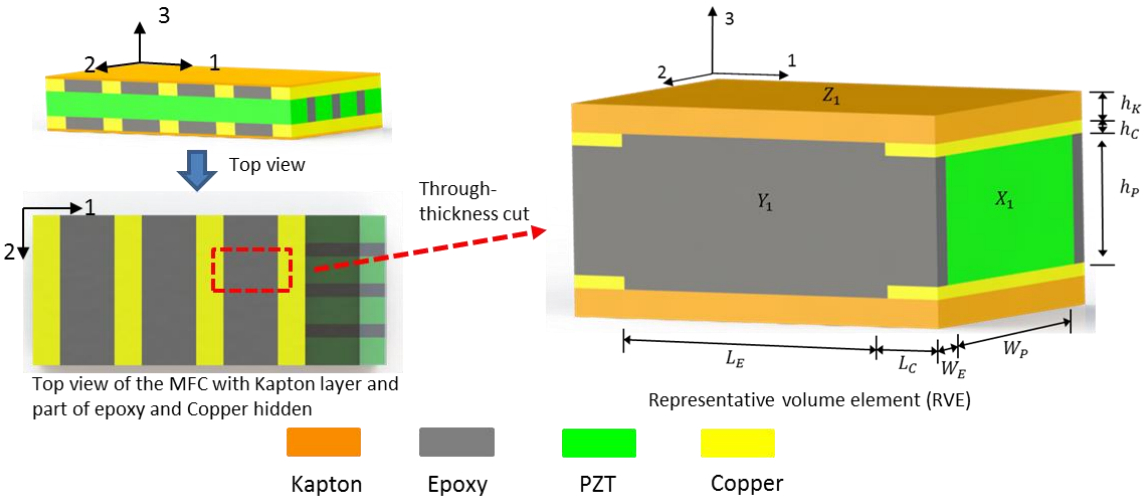


Fig. 3 The representative volume element (RVE) of the $d_{31}$ type MFC obtained by a through-thickness cut, which represents the minimum periodic unit of an MFC

An FE model of the RVE was developed in COMSOL Multiphysics®. The dimensions of the RVE are listed in Table 1 and the material properties of the MFC constituents are listed in Table 2. Of the dimensions, the copper width $L_C$ was estimated by microphotography of the MFC in [23] and represents a volume fraction of 27.6% in the copper/epoxy layer; others are in accordance with the dimensions of the standard $d_{31}$ MFCs produced by Smart Material Corp., which have a PZT fiber volume fraction of 86% in the active layer. The material properties of the PZT fibres (PZT5A1) are adopted from [16]. The dielectric constant of the epoxy (relative permittivity: 4.25 [23]) was not considered because it is negligible compared to that of the PZT fiber (relative permittivity:1850). The FE model of the RVE with meshes is shown in Fig. 4.

Table 1 Dimensions of the representative volume element of the $d_{31}$ MFC

| Dimension | Value | Dimension | Value | Dimension | Value | Dimension | Value |
|---|---|---|---|---|---|---|---|
| $L_E$ (μm) | 420 | $L_C$ (μm) | 80 | $W_E$ (μm) | 28.35 | $W_P$ (μm) | 348.3 |
| $h_K$ (μm) | 40 | $h_C$ (μm) | 18 | $h_P$ (μm) | 185 | | |

Table 2 Material properties of the MFC constitutes

| Properties | PZT fibre | Epoxy | Copper | Kapton |
|---|---|---|---|---|
| Young's modulus (GPa) | $Y_1$=$Y_2$=54.05; $Y_3$=48.30 | 2.5 | 110 | 2.5 |
| Shear modulus (GPa) | $G_{23}$=$G_{13}$=29.41; $G_{12}$=19.14 | - | - | - |
| Poisson's ratio | $v_{23}$=$v_{13}$=0.38; $v_{12}$=0.41 | 0.42 | 0.34 | 0.34 |
| Piezoelectric constants (pC/N) | $d_{31}$=$d_{32}$=-185; $d_{33}$=440 | - | - | - |
| Relative permittivity | $\varepsilon_{11}^T$=$\varepsilon_{22}^T$=1902; $\varepsilon_{33}^T$=1850 | - | - | - |

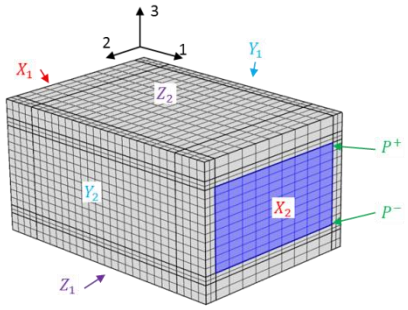


Fig. 4 the FE model of the RVE with the PZT fibre highlighted in blue

In the FE model, electric boundary conditions were applied to the two boundary surfaces of the PZT fibre, which are normal to 3-axis and denoted as $P^+$ and $P^-$ in Fig. 4. Displacement boundary conditions were applied to the six boundary surfaces of the cubic RVE: $X_1$, $X_2$, $Y_1$, $Y_2$, $Z_1$ and $Z_2$. Of these surfaces, $X_1$ and $X_2$ are normal to 1-axis; $Y_1$ and $Y_2$ are normal to 2-axis; $Z_1$ and $Z_2$ are normal to 3-axis.

### 3.2 Periodic boundary conditions and equation solving

To facilitate the solving of Eq. ( 2 ), seven sets of periodic boundary conditions (BCs) were created for the FE model. These BCs follows the methods described in [19, 23] and are listed in Table 3, where $u_q(K)$ with $q = 1,2,3$ and $K = X_1, X_2, Y_1, Y_2, Z_1, Z_2$ is the displacement of the surface $K$ along $q$-axis; $E(P)$ with $P = P^+, P^-$ is the electric potential on surface $P$. $k$ and $p$ are arbitrary values of displacement and voltage, respectively. They were assigned as $60\times10^{-9}$ m and 1 V, respectively in this study.

The seven sets of BCs were designed so that some values of $\bar{T}_j$, $\bar{S}_j$, $\bar{Q}_3$ and $\bar{U}_3$ were zero to enable the solving of Eq. ( 2 ). For each BC set, the FE model simulated the static responses ($\check{S}_j$, $\check{T}_j$, $\check{Q}_3$ and $\check{U}_3$ ) of the RVE. Then $\bar{T}_j$, $\bar{S}_j$, $\bar{Q}_3$ and $\bar{U}_3$ were evaluated according to Eq. ( 5 ) and ( 4 ). Finally, the values of $\bar{T}_j$, $\bar{S}_j$, $\bar{Q}_3$ and $\bar{U}_3$ were substituted to Eq. ( 2 ) to calculate the equivalent properties.

In the BC set $n$, $n = 1,2,3$, the RVE was constrained to a short-circuit condition by applying zero electric potential to both electrodes so that $\bar{U}_3 = 0$. The displacement constraints were applied in such a way that only one normal strain was present ($\bar{S}_j \neq 0, j = n$) while the other two normal strains were zero ($\bar{S}_j = 0, j \neq n$), as shown in the 'resultant inputs' column of Table 3. Substituting the values of $\bar{S}_j$, $\bar{T}_j$, $\bar{U}_3$ and $\bar{Q}_3$ into Eq. ( 2 ), the following elastic constants and piezoelectric stress constants can be solved

$$\bar{c}_{jn} = \frac{\bar{T}_j}{\bar{S}_n}, \bar{e}_{3n} = \frac{\bar{Q}_3}{\bar{A}_e \bar{S}_n} \qquad n, j = 1,2,3. \tag{9}$$

When $n = 4,5,6$, the RVE was constrained to a short-circuit condition by applying zero electric potential to both electrodes so that $\bar{U}_3 = 0$. The displacement was applied in such a way that a pure shear strain $\bar{S}_n$ was produced in the

RVE. With the shear stress $\bar{T}_n$ derived from the FE analysis, the equivalent elastic parameters related to the shear stress/strain were calculated by solving Eq. ( 2 ) as

$$\bar{c}_{nn} = \frac{\bar{T}_n}{\bar{S}_n} \qquad n = 4,5,6. \tag{10}$$

For BC set 7, the displacements in all directions were constrained to zero to block the strains in all directions so that $\bar{S}_1 = \bar{S}_2 = \bar{S}_3 = 0$. A voltage $\bar{U}_3$ was applied across electrodes $P^-$ and $P^+$. With $\bar{Q}_3$ derived from the FE analysis, the dielectric constant was calculated by solving Eq. ( 2 )

$$\bar{\epsilon}_{33}^S = \frac{\bar{Q}_3 \bar{t}_e}{\bar{A}_e \bar{U}_3} \tag{11}$$

Table 3 The boundary conditions input to the FE model and the routine to solve Eq. ( 2 )

| Set | Boundary Conditions | | | | Resultant inputs | Resultant outputs | Solutions of |
|---|---|---|---|---|---|---|---|
| $n$ | $X_1/X_2$ | $Y_1/Y_2$ | $Z_1/Z_2$ | $P^+/P^-$ | | | Eq. ( 2 ) |
| 1 | $u_1(X_1) = 0$<br>$u_1(X_2) = k$ | $u_2(Y_1) = 0$<br>$u_2(Y_2) = 0$ | $u_3(Z_1) = 0$<br>$u_3(Z_2) = 0$ | $E(P^+)$=0<br>$E(P^-)$=0 | $\bar{S}_1 \neq 0$<br>$\bar{S}_2 = \bar{S}_3 = 0$<br>$\bar{U}_3 = 0$ | $\bar{T}_j \quad j = 1,2,3$<br>$\bar{Q}_3$ | $\bar{c}_{j1}^E = \bar{T}_j/\bar{S}_1$<br>$\bar{e}_{31} = \bar{Q}_3/\bar{A}_e\bar{S}_1$ |
| 2 | $u_1(X_1) = 0$<br>$u_1(X_2) = 0$ | $u_2(Y_1) = 0$<br>$u_2(Y_2) = k$ | $u_3(Z_1) = 0$<br>$u_3(Z_2) = 0$ | $E(P^+)$=0<br>$E(P^-)$=0 | $\bar{S}_2 \neq 0$<br>$\bar{S}_1 = \bar{S}_3 = 0$<br>$\bar{U}_3 = 0$ | $\bar{T}_j \quad j = 1,2,3$<br>$\bar{Q}_3$ | $\bar{c}_{j2}^E = \bar{T}_j/\bar{S}_2$<br>$\bar{e}_{32} = \bar{Q}_3/\bar{A}_e\bar{S}_2$ |
| 3 | $u_1(X_1) = 0$<br>$u_1(X_2) = 0$ | $u_2(Y_1) = 0$<br>$u_2(Y_2) = 0$ | $u_3(Z_1) = 0$<br>$u_3(Z_2) = k$ | $E(P^+)$=0<br>$E(P^-)$=0 | $\bar{S}_3 \neq 0$<br>$\bar{S}_2 = \bar{S}_3 = 0$<br>$\bar{U}_3 = 0$ | $\bar{T}_j \quad j = 1,2,3$<br>$\bar{Q}_3$ | $\bar{c}_{j3}^E = \bar{T}_j/\bar{S}_3$<br>$\bar{e}_{33} = \bar{Q}_3/\bar{A}_e\bar{S}_3$ |
| 4 | $u_1(X_1) = 0$<br>$u_1(X_2) = 0$ | $u_3(Y_1) = -k$<br>$u_3(Y_2) = k$ | $u_2(Z_1) = k$<br>$u_2(Z_2) = -k$ | $E(P^+)$=0<br>$E(P^-)$=0 | $\bar{S}_4 \neq 0$<br>$\bar{U}_3 = 0$ | $\bar{T}_4$ | $\bar{c}_{44}^E = \bar{T}_4/\bar{S}_4$ |
| 5 | $u_3(X_1) = -k$<br>$u_3(X_2) = k$ | $u_2(Y_1) = 0$<br>$u_2(Y_2) = 0$ | $u_1(Z_1) = k$<br>$u_1(Z_2) = -k$ | $E(P^+)$=0<br>$E(P^-)$=0 | $\bar{S}_5 \neq 0$<br>$\bar{U}_3 = 0$ | $\bar{T}_5$ | $\bar{c}_{55}^E = \bar{T}_5/\bar{S}_5$ |
| 6 | $u_2(X_1) = -k$<br>$u_2(X_2) = k$ | $u_1(Y_1) = k$<br>$u_1(Y_2) = k$ | $u_3(Z_1) = 0$<br>$u_3(Z_2) = 0$ | $E(P^+)$=0<br>$E(P^-)$=0 | $\bar{S}_6 \neq 0$<br>$\bar{U}_3 = 0$ | $\bar{T}_6$ | $\bar{c}_{66}^E = \bar{T}_6/\bar{S}_6$ |
| 7 | $u_1(X_1) = 0$<br>$u_1(X_2) = 0$ | $u_2(Y_1) = 0$<br>$u_2(Y_2) = 0$ | $u_3(Z_1) = 0$<br>$u_3(Z_2) = 0$ | $E(P^+) = p$<br>$E(P^-)$=0 | $\bar{S}_1 = \bar{S}_2 = \bar{S}_3$<br>$= 0$<br>$\bar{U}_3 \neq 0$ | $\bar{Q}_3$ | $\bar{\epsilon}_{33}^S$<br>$= \bar{Q}_3\bar{t}_e/\bar{A}_e\bar{U}_3$ |

### 3.3 Evaluated equivalent properties

The equivalent properties of the MFC evaluated in this study are listed in Table 4. The piezoelectric strain constants were converted by using Eq. ( 12 ). Other piezoelectric stress constants ($\bar{e}_{15}, \bar{e}_{24}$) and dielectric constants ($\bar{\epsilon}_{11}^S, \bar{\epsilon}_{22}^S$) are difficult to evaluate from a piezoelectric material polled along 3-axis. They do not affect the performance of the d31-type MFC and therefore can be specified with any reasonable values to complete the property matrix when needed in FE modelling. For the following sections, they are specified with the corresponding parameters of the PZT.

$$\begin{bmatrix} \bar{d}_{31} \\ \bar{d}_{32} \\ \bar{d}_{33} \end{bmatrix} = \begin{bmatrix} \bar{c}_{11}^E & \bar{c}_{12}^E & \bar{c}_{13}^E \\ \bar{c}_{21}^E & \bar{c}_{22}^E & \bar{c}_{23}^E \\ \bar{c}_{31}^E & \bar{c}_{32}^E & \bar{c}_{33}^E \end{bmatrix}^{-1} \begin{bmatrix} \bar{e}_{31} \\ \bar{e}_{32} \\ \bar{e}_{33} \end{bmatrix} \tag{12}$$

Table 4 Equivalent properties of the homogeneous MFC

| Property | value | Property | value | Property | value | Property | value | Property | value |
|---|---|---|---|---|---|---|---|---|---|
| $\bar{c}_{11}^E$(GPa) | 37.60 | $\bar{c}_{12}^E$(GPa) | 10.70 | $\bar{c}_{13}^E$(GPa) | 5.87 | $\bar{e}_{31}$ (C/m$^2$) | -10.0 | $\bar{d}_{31}$ (pC/N) | -283.4 |

| | | | | | | | | | |
|---|---|---|---|---|---|---|---|---|---|
| $\bar{c}_{21}^{E}$(GPa) | 10.70 | $\bar{c}_{22}^{E}$(GPa) | 24.08 | $\bar{c}_{23}^{E}$(GPa) | 5.12 | $\bar{e}_{32}$ (C/m$^2$) | -5.78 | $\bar{d}_{32}$(pC/N) | -223.2 |
| $\bar{c}_{31}^{E}$(GPa) | 5.87 | $\bar{c}_{32}^{E}$(GPa) | 5.12 | $\bar{c}_{33}^{E}$(GPa) | 10.51 | $\bar{e}_{33}$ (C/m$^2$) | 2.59 | $\bar{d}_{33}$(pC/N) | 513.4 |
| $\bar{c}_{44}^{E}$(GPa) | 2.21 | $\bar{c}_{55}^{E}$(GPa) | 2.50 | $\bar{c}_{66}^{E}$(GPa) | 5.41 | $\bar{\epsilon}_{33}^{S}/\epsilon_0$ | 1935 | | |

# 4. Validation of the equivalent properties for energy harvesting transducer modelling

## 4.1 Validation by comparing the power outputs of the heterogeneous and homogenous RVEs

Since the equivalent properties were derived based on a heterogeneous RVE, the energy harvesting performance of a homogeneous RVE should approximate that of the heterogeneous RVE. This will be verified by comparing the simulated power outputs of the heterogeneous and homogeneous RVEs.

### 4.1.1 FE modelling of the RVEs for energy harvesting

The FE models of heterogeneous and homogeneous RVEs for energy harvesting were developed in COMSOL Multiphysics®, as shown in Fig. 5. The heterogeneous RVE used the same structure and material properties as Section 3. A load resistor was connected to the electrodes of the PZT fibre, which are $P^+$ and $P^-$, to collect the electric voltage. The homogeneous RVE had the same boundary dimensions as the heterogeneous RVE and was specified with the equivalent properties listed Table 4. The load resistor was connected to the two boundary surfaces normal to 3-axis. For both RVEs, the boundary surface $X_1$ was constrained for displacement along 1-axis, while a sinusoidal force or displacement was applied on the surface $X_2$ along 1-axis. Harmonic analysis was performed at a frequency of 10 Hz. The voltage amplitude and the average electric power in the load resistors were recorded.

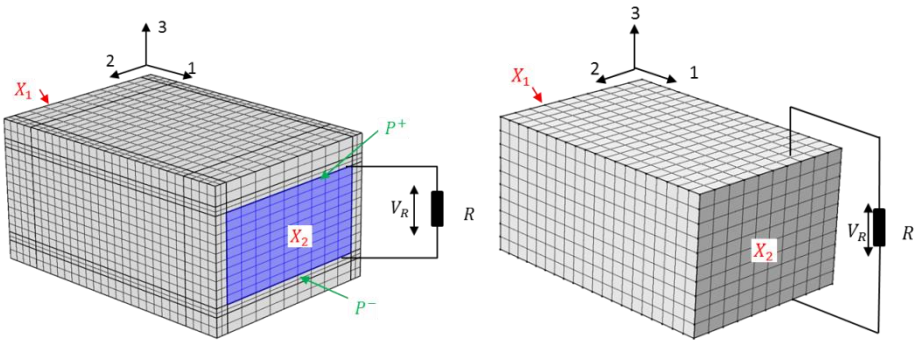


(a) (b)

Fig. 5 The FE model of (a) the heterogeneous RVE and (b) homogeneous RVE for energy harvesting

### 4.1.2 Results and Discussions

Fig. 6 presents the voltage and average power output of the RVEs as a function of the load resistance when a displacement of 0.174 $\mu m$ was applied. The electric outputs of the homogenous RVE agree well with those of the heterogeneous RVE. Both RVEs showed a maximum power output of 0.38 μW when the load resistance is 1000 MΩ. This resistance is the optimal load resistance of the RVEs and equals the internal impedance of the RVEs resulted from the intrinsic capacitance ($\bar{C}_P^S$=1.5×10$^{-11}$ Farad). The maximum power outputs of the RVEs as a function of strains and forces are presented in Fig. 7. Good agreement in the power outputs is observed at different strains and forces, although there is a slight discrepancy up to 5.4% when a force is applied.

The good agreement in the power outputs of the heterogeneous and homogeneous RVEs suggests that the equivalent properties describe accurately the energy harvesting behaviours of the heterogeneous RVEs. Although these equivalent properties were obtained with restrictions in strains, they can also be used when force/stress is applied.

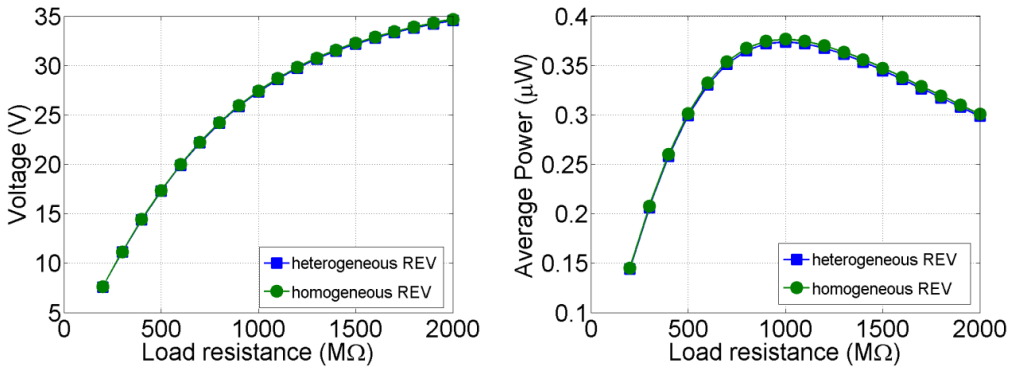


(a) (b)

Fig. 6 (a) voltages and (b) power outputs produced by the heterogeneous and homogeneous RVEs subjected to a sinusoidal displacement of 0.174 $\mu m$ at 10 Hz

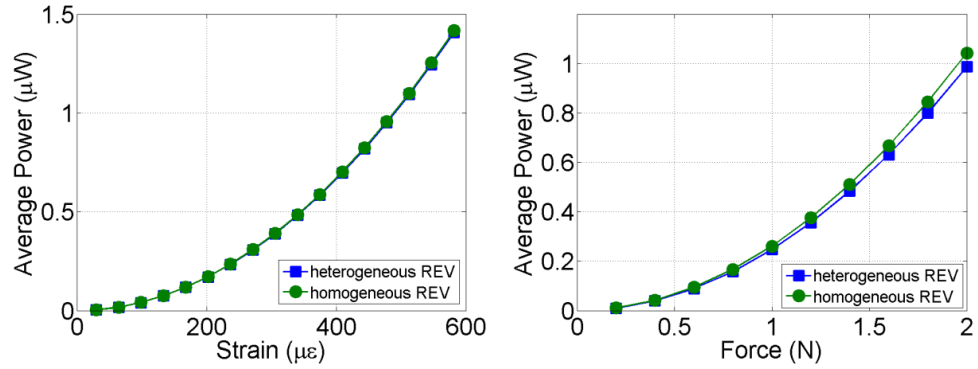


(a) (b)

Fig. 7 Power outputs of the heterogeneous and homogeneous RVEs at (a) different load strains and (b) different load forces

**4.2 Validation by comparing the simulated and measured power outputs of MFC-based strain energy harvesters**

Following validating equivalent properties on RVEs, the power outputs of MFC-based strain energy harvesters (SEHs) were simulated and compared with experimental results.

4.2.1 Strain energy harvesters and experimental setup

The strain energy harvester (Fig. 8) was designed and fabricated to harvest energy from engineering structures undergoing dynamic strains. It consists of a $d_{31}$ MFC (M8528-P2, dimensions: 85×28×0.3 $mm^3$, Smart Material Corp.) adhesively bonded to a substrate. During fabrication, the surface of the substrate was processed by a sandpaper to improve the bonding quality. Adhesive epoxy (Araldite® 2014-1) was applied to the substrate and then the MFC was attached. The substrate and the MFC were then sealed within a vacuum bag and cured at 70 ºC for 3 hours with a pressure of 60 psi applied by an autoclave. Metal studs were boned to the end portion of the substrate to facilitate clamping and applying dynamic strains.

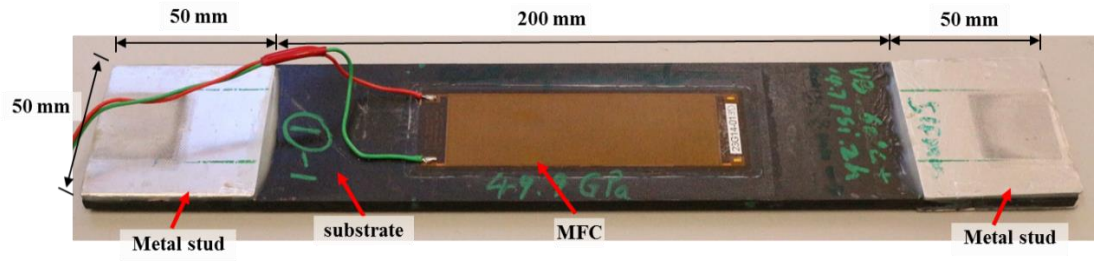

Fig. 8 the strain energy harvester used for this study

The SEH was tested on a material testing machine (Instron ElectroPlus E10000), as shown Fig. 9. The material testing machine clamped the SEH through the metal studs. An extensometer was used to measure the strain developed in the substrate. The material testing machine applied a bipolar sinusoidal force on the SEH, which takes the form of

$$F = F_s + F_a \sin(2\pi f t). \quad (13)$$

$F_s$ is a static force, which ensures that the SEH is always in tension during the test to avoid buckling. $F_a$ and $f$ are the amplitude and frequency of the applied dynamic force. The value of $F_a$ was adjusted until the measured dynamic strain in the substrate reached at the desired value. A variable load resistor was connected to the electrodes of the MFC, and the voltage across the load resistor was recorded to calculate the generated electric power. In total five SEHs were fabricated and tested.

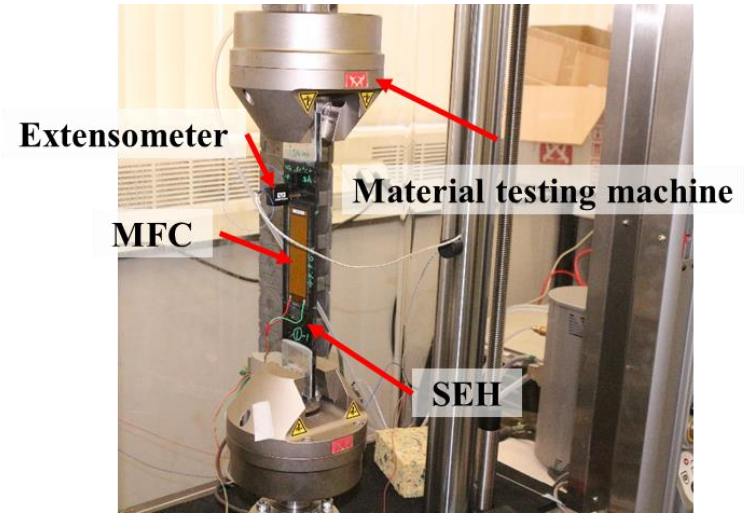


Fig. 9 The experimental setup for testing the strain energy harvesters

4.2.2 FE modelling of the SEH

An FE model of the SEH was developed in COMSOL Multiphysics®, as shown in Fig. 10. The MFC was modelled as a homogeneous material with the equivalent properties (Table 4) and dimensions of 85×28×0.3 mm3. A load resistor was connected to the two normal-to-3-axis boundary surfaces of the MFC. To simulate the load applied in the experiment, one end of the substrate (200×50×5 mm3) was fixed, while a sinusoidal displacement load was applied on the other end so that the strain in the substrate was the same as the experiment.

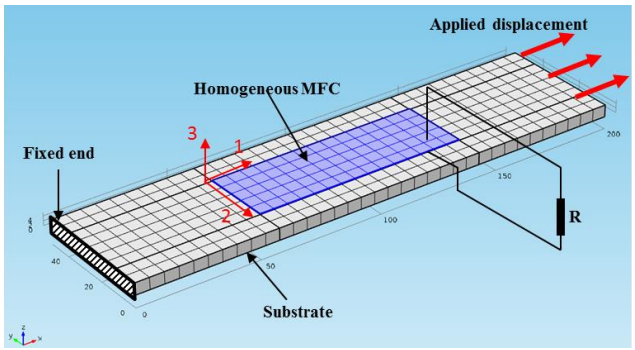


Fig. 10 A schematic of the FE model of the strain energy harvester developed in COMSOL

4.2.3 Comparison between the FE modelling and experiment

The measured power outputs of the SEHs are compared with the simulated in Fig. 11. The measured power outputs are presented as the mean values of the five samples with standard deviations. The strain amplitude in both simulation and experiment is 100 με. The simulated power outputs coincide with the mean values of the measured outputs. The FE model predicted a maximum power of 0.40 mW with an optimal load resistance of 100 kΩ, while the experiment showed a maximum power of 0.41±0.05 mW at 90 kΩ. The error in the power output prediction is 2.5%.

It is noted that the measured power outputs of the five SEHs deviate from the mean value by up to 12.1%. The variation is likely because of the deviations in the material properties and fibre volume fractions of the MFCs. The properties of the PZT usually vary by up to ±5-10% of the values provided by the supplier, which can lead to the deviations in the power output. Moreover, although the same fabrication process was used, the amount and thickness of the adhesive layer and thus the bonding quality was difficult to keep consistent and is expected to partly cause the deviation in the power output.

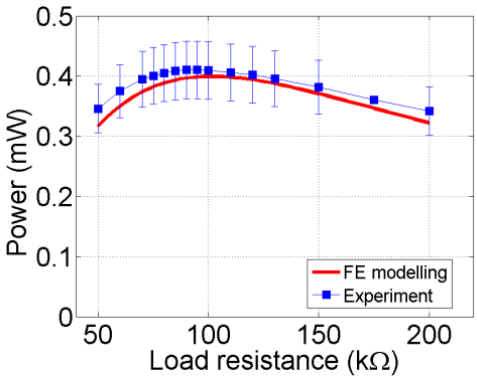


Fig. 11 Comparison of the simulated and measured power output of the strain energy harvester with a dynamic strain of 100 $\mu\varepsilon$ at 10 Hz

When a strain of 300 $\mu\varepsilon$ was applied at different frequencies, the simulated and measured performance is compared in Fig. 12. The FE modelling predicted the maximum power and the optimal load resistance with satisfactory accuracy.

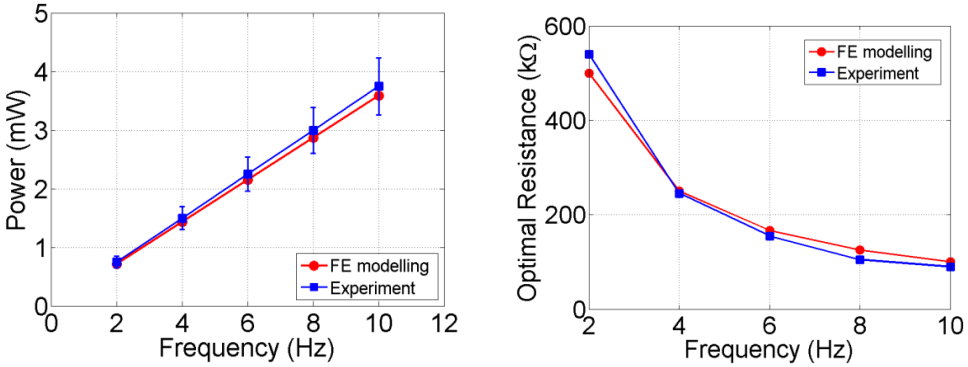


Fig. 12 Comparison of the simulated and measured performance of the SEHs at different frequencies: (a) the maximum power output and (b) the optimal load resistance

## 5. Applications of the equivalent properties for sensing and actuation transducers

When a piezoelectric transducer is used for sensing, the piezoelectric material produces an open-circuit voltage proportional to the strain or force applied to the transducer [32]. Because the open-circuit voltages of the heterogeneous and homogeneous MFCs are kept equal during the homogenisation process in this study, the equivalent properties can naturally be used for modelling MFC-based sensing transducers.

To validate the application of the equivalent properties for actuation transducer modelling, the FE models of RVEs in Fig. 5 were modified: a voltage of 1 V was applied to the electrodes instead of connecting a load resistor to the electrodes. Other conditions were kept unchanged. The heterogeneous and homogenous RVE showed an average strain $S_1$ of 0.92

$\mu\varepsilon$ and 0.94 $\mu\varepsilon$, respectively. This suggests that the equivalent properties can approximate the actuation behaviour of the heterogeneous RVE. Further, the free strain generated by the homogenous MFC with 1 volt applied can be calculated as

$$\bar{S}_{1f} = \frac{\bar{d}_{31}}{\bar{t}_e} \quad (14)$$

The result is compared in Table 5 with the manufacturer datasheet and the value estimated by Steiger [28]. The free strain estimated by the equivalent properties in this study is quite close to the manufacturer datasheet and is slightly superior to the result in [28]. Therefore, the equivalent properties evaluated in this study can also be used for MFC-based actuation transducer modelling.

Table 5 Comparison of the free strains calculated using the equivalent properties in this study, estimated by Steiger [28] and provided by the manufacturer datasheet (unit: microstrain per volt)

| Present study | Steiger's work [28] | Manufacturer datasheet |
|---|---|---|
| 0.95 | 0.89 | 1.1 |

## 6. Conclusions

In this work, an equal power method was proposed for the first time to evaluate the equivalent properties of macro fibre composite for piezoelectric transducer modelling. Instead of using the traditional electrical assumption of average quantity, a new assumption was introduced to ensure the equality of the electrical charge, voltage and capacitance of the heterogeneous and homogenous MFCs. The proposed homogenization procedure was implemented with the aid of finite element analysis on the representative volume element of the MFC. The validity of these equivalent properties for energy harvesting transducer modelling was verified by two steps. Firstly, the energy harvesting performance of a homogeneous RVE with the derived equivalent properties was compared with that of the heterogeneous RVE. The good agreement suggests that the equivalent properties describe accurately the energy harvesting behaviours of the MFC. Secondly, a finite element model of an MFC-based strain energy harvester was developed, and the simulated power output was compared with experimental results. The finite element model is able to predict the power output of the strain energy harvesters with an error of 2.5%. The evaluated properties can also be used for sensing transducer modelling because a piezoelectric sensing transducer measures the open-circuit voltage produced due to an applied stress/strain while the proposed homogenization maintains the equality of the voltage produced by the heterogeneous and homogeneous MFCs. The homogenised MFC produced a free strain close to the manufacturer specification, validating its application for actuation transducer modelling.

## Acknowledgement

The authors gratefully acknowledge financial support from the Engineering and Physical Sciences Research Council (EPSRC) in the UK through funding of the research into 'En-ComE-Energy Harvesting Powered Wireless Monitoring Systems Based on Integrated Smart Composite Structures and Energy-aware Architecture' (EP/K020331/1).

## References

[1] Y. Kuang and M. Zhu, "Characterisation of a knee-joint energy harvester powering a wireless communication sensing node," *Smart Materials & Structures*, 2016.

[2] Y. Kuang, T. Ruan, Z. J. Chew, and M. Zhu, "Energy harvesting during human walking to power a wireless sensor node," *Sensors and Actuators A: Physical*, vol. 254, pp. 69-77, 2/1/ 2017.

[3] C. Niezrecki, D. Brei, S. Balakrishnan, and A. Moskalik, "Piezoelectric actuation: state of the art," 2001.

[4] C. R. Bowen, P. F. Giddings, A. I. Salo, and H. A. Kim, "Modeling and characterization of piezoelectrically actuated bistable composites," *IEEE transactions on ultrasonics, ferroelectrics, and frequency control*, vol. 58, pp. 1737-1750, 2011.

[5] X. Zhao, T. Qian, G. Mei, C. Kwan, R. Zane, C. Walsh, *et al.*, "Active health monitoring of an aircraft wing with an embedded piezoelectric sensor/actuator network: II. Wireless approaches," *Smart materials and structures*, vol. 16, p. 1218, 2007.

[6] S. R. Anton and H. A. Sodano, "A review of power harvesting using piezoelectric materials (2003–2006)," *Smart Materials and Structures*, vol. 16, p. R1, 2007.

[7] K. Yang, Y. Zhihao, and Z. Meiling, "Design and characterisation of a piezoelectric knee-joint energy harvester with frequency up-conversion through magnetic plucking," *Smart Materials and Structures*, vol. 25, p. 085029, 2016.
[8] H. Li, C. Tian, and Z. D. Deng, "Energy harvesting from low frequency applications using piezoelectric materials," *Applied Physics Reviews*, vol. 1, p. 041301, 2014.
[9] J. J. Zhao and Z. You, "A Shoe-Embedded Piezoelectric Energy Harvester for Wearable Sensors," *Sensors*, vol. 14, pp. 12497-12510, Jul 2014.
[10] P. F. Giddings, H. A. Kim, A. I. Salo, and C. R. Bowen, "Modelling of piezoelectrically actuated bistable composites," *Materials Letters*, vol. 65, pp. 1261-1263, 2011.
[11] D. N. Betts, H. A. Kim, C. R. Bowen, and D. Inman, "Optimal configurations of bistable piezo-composites for energy harvesting," *Applied Physics Letters*, vol. 100, p. 114104, 2012.
[12] Z. J. Chew, T. Ruan, M. Zhu, M. Bafleur, and J.-M. Dilhac, "Single Piezoelectric Transducer as Strain Sensor and Energy Harvester Using Time-multiplexing Operation," *IEEE Transactions on Industrial Electronics*, 2017.
[13] A. Erturk, M. I. Friswell, S. F. Ali, O. Bilgen, S. Adhikari, A. W. Lees, *et al.*, "Non-linear piezoelectric vibration energy harvesting from a vertical cantilever beam with tip mass," *Journal of Intelligent Material Systems and Structures*, vol. 23, pp. 1505-1521, 2012.
[14] (accessed in Dec 2017). *https://www.smart-material.com/media/Datasheets/MFC_V2.3-Web-full-brochure.pdf*.
[15] A. Deraemaeker, H. Nasser, A. Benjeddou, and A. Preumont, "Mixing rules for the piezoelectric properties of macro fiber composites," *Journal of intelligent material systems and structures*, vol. 20, pp. 1475-1482, 2009.
[16] A. Deraemaeker, S. Benelechi, A. Benjeddou, and A. Preumont, "Analytical and numerical computation of homogenized properties of MFCs: Application to a composite boom with MFC actuators and sensors," in *Proceedings of the III ECCOMAS thematic conference on Smart Structures and Materials*, 2007.
[17] H. Berger, S. Kari, U. Gabbert, R. Rodriguez-Ramos, R. Guinovart, J. A. Otero, *et al.*, "An analytical and numerical approach for calculating effective material coefficients of piezoelectric fiber composites," *International Journal of Solids and Structures*, vol. 42, pp. 5692-5714, 2005.
[18] S. S. Prasath and A. Arockiarajan, "Effective electromechanical response of macro-fiber composite (MFC): Analytical and numerical models," *International Journal of Mechanical Sciences*, vol. 77, pp. 98-106, 2013.
[19] S. S. Prasath and A. Arockiarajan, "Analytical, numerical and experimental predictions of the effective electromechanical properties of macro-fiber composite (MFC)," *Sensors and Actuators A: Physical*, vol. 214, pp. 31-44, 2014.
[20] F. Biscani, H. Nasser, S. Belouettar, and E. Carrera, "Equivalent electro-elastic properties of Macro Fiber Composite (MFC) transducers using asymptotic expansion approach," *Composites Part B: Engineering*, vol. 42, pp. 444-455, 2011.
[21] M. Trindade and A. Benjeddou, "Finite element homogenization technique for the characterization of d15 shear piezoelectric macro-fibre composites," *Smart Materials and Structures*, vol. 20, p. 075012, 2011.
[22] B. Kranz, A. Benjeddou, and W.-G. Drossel, "Numerical and experimental characterizations of longitudinally polarized piezoelectric d^ sub 15^ shear macro-fiber composites," *Acta Mechanica*, vol. 224, p. 2471, 2013.
[23] M. A. Trindade and A. Benjeddou, "Finite element characterisation of multilayer d31 piezoelectric macro-fibre composites," *Composite Structures*, 2015.
[24] A. Deraemaeker and H. Nasser, "Numerical evaluation of the equivalent properties of Macro Fiber Composite (MFC) transducers using periodic homogenization," *International journal of solids and structures*, vol. 47, pp. 3272-3285, 2010.
[25] S. S. Prasath and A. Arockiarajan, "Influence of bonding layer on effective electromechanical properties of macro-fiber composites (MFCs)," *Smart Materials and Structures*, vol. 23, p. 095046, 2014.
[26] M. A. Trindade and A. Benjeddou, "Finite Element Techniques for the Characterization of Effective Properties of Transverse Piezoelectric Macro-fiber Composites " presented at the 8th VIII ECCOMAS Thematic Conference on Smart Structures and Materials, Madrid, Spain, 2017.
[27] B. Kranz, A. Benjeddou, and W.-G. Drossel, "Enthalpy-based homogenization procedure for composite piezoelectric modules with integrated electrodes," *Smart Structures and Systems*, vol. 12, pp. 579-594, 2013.
[28] K. Steiger and P. Mokrý, "Finite element analysis of the macro fiber composite actuator: macroscopic elastic and piezoelectric properties and active control thereof by means of negative capacitance shunt circuit," *Smart Materials and Structures*, vol. 24, p. 025026, 2015.
[29] S. Roundy, P. K. Wright, and J. Rabaey, "A study of low level vibrations as a power source for wireless sensor nodes," *Computer communications*, vol. 26, pp. 1131-1144, 2003.
[30] T.-B. Xu, E. J. Siochi, J. H. Kang, L. Zuo, W. Zhou, X. Tang, *et al.*, "Energy harvesting using a PZT ceramic multilayer stack," *Smart Materials and Structures*, vol. 22, p. 065015, 2013.
[31] P. Tan and L. Tong, "Micro-electromechanics models for piezoelectric-fiber-reinforced composite materials," *Composites science and technology*, vol. 61, pp. 759-769, 2001.
[32] J. Sirohi and I. Chopra, "Fundamental understanding of piezoelectric strain sensors," *Journal of Intelligent Material Systems and Structures*, vol. 11, pp. 246-257, 2000.